ELSEVIER

Journal of Hazardous Materials B138 (2006) 560–573

Journal of Hazardous Materials

www.elsevier.com/locate/jhazmat

Performance estimation of a Venturi scrubber using a computational model for capturing dust particles with liquid spray

S.I. Pak [a,*], K.S. Chang [b]

[a] *National Fusion Research Center, 52 Eoeun-dong, Yuseong-gu, Daejeon 305-333, Republic of Korea*
[b] *Department of Aerospace Engineering, KAIST, Daejeon, Republic of Korea*

Received 5 January 2006; received in revised form 18 May 2006; accepted 28 May 2006
Available online 16 June 2006

Abstract

A Venturi scrubber has dispersed three-phase flow of gas, dust, and liquid. Atomization of a liquid jet and interaction between the phases has a large effect on the performance of Venturi scrubbers. In this study, a computational model for the interactive three-phase flow in a Venturi scrubber has been developed to estimate pressure drop and collection efficiency. The Eulerian–Lagrangian method is used to solve the model numerically. Gas flow is solved using the Eulerian approach by using the Navier-Stokes equations, and the motion of dust and liquid droplets, described by the Basset–Boussinesq–Oseen (B–B–O) equation, is solved using the Lagrangian approach. This model includes interaction between gas and droplets, atomization of a liquid jet, droplet deformation, breakup and collision of droplets, and capture of dust by droplets. A circular Pease–Anthony Venturi scrubber was simulated numerically with this new model. The numerical results were compared with earlier experimental data for pressure drop and collection efficiency, and gave good agreements.

Keywords: Venturi scrubber; Dispersed three-phase flow; Eulerian–Lagrangian method; Computational model

1. Introduction

Micron-sized dust particles are known to have a fatal effect on human bodies, especially the heart and lungs. These fine particles are mainly generated from the internal combustion engines of cars and other motor vehicles, fuel burned at stationary sources such as power-generating plants, and various other industrial processes. A lot of Venturi scrubbers have been used in industrial plants, starting in the 1940s, to remove the harmful dust particles.

Venturi scrubbers are very high in collection efficiency while the establishment and maintenance costs are low. The dust that the devices can remove is between 0.5∼10 μm in diameter. Fig. 1 shows how the system of a Venturi scrubber is composed. A Venturi scrubber consists of three parts: convergence, throat, and diffuser. The dust particles introduced with the air are accelerated in the convergence and collide with the liquid droplets at the throat, mainly through inertial impaction. The other collision mechanisms, such as interception and Brownian diffusion, also work, but they are very weak in comparison with the inertial impaction [1]. The droplets that captured the dust particles are separated at the cyclone separator, connected to the Venturi scrubber, and go out through the drain hole. The clean air is discharged into the atmosphere and the drained liquid is treated for reuse. This process is drawn in Fig. 1.

Venturi scrubbers can be classified as either the liquid injection type (Pease–Anthony type) or the wetted approach type according to how the liquid is supplied [2]. In the former type, the liquid is injected from the orifices located on the Venturi throat as shown Fig. 1. The injected liquid jet breaks up into small droplets by aerodynamic force. The latter device introduces the liquid from the convergence part of the Venturi, and the liquid flows as liquid film along the wall. At the throat, the liquid sheds the droplets by the shear action of aerodynamic force. In this paper we studied the Pease–Anthony type of Venturi scrubber.

The performance of the gas cleaning equipment has been evaluated by means of pressure drop and collection efficiency. The pressure drop is directly related to the operational cost. The

* Corresponding author. Tel.: +82 42 870 1635; fax: +82 42 870 1939.
E-mail addresses: paksunil@dreamwiz.com (S.I. Pak), kschang@kaist.ac.kr (K.S. Chang).

0304-3894/$ – see front matter © 2006 Elsevier B.V. All rights reserved.
doi:10.1016/j.jhazmat.2006.05.105

Nomenclature

A_p	frontal particle (droplet or dust) area perpendicular to gas stream (m^2)
C_D	drag coefficient of particle (dimensionless)
d_0	initial droplet diameter (m)
d_d	droplet diameter (m)
d_{def}	diameter of deformed droplet due to aerodynamic force (m)
d_s	density of dust particle (m)
d_V	volume of a computational cell (m^3)
D_{32}	Sauter mean diameter of droplets (m)
$D_{84\%}$	diameter corresponding to the 84^{th} percentile (m)
D_M	median diameter (m)
k	turbulent kinetic energy (m^2/s^2)
l/g	liquid-to-gas volume flow ratio (l/m^3)
m_p	particle mass (kg)
N_{cap}	number of dust particles captured by one droplet parcel
N_{cell}	total number of dust particles absorbed by all droplets within a computational cell
N_d	number of particles represented by one droplet parcel
N_s	number of particles represented by one dust parcel
Oh	Ohnesorge number (dimensionless)
r/R_{max}	radial distance from throat center of Venturi (dimensionless)
Re_d	droplet Reynolds number (dimensionless)
Re_s	Reynolds number of dust particle (dimensionless)
$S_{\phi,p}$	source term due to interaction with droplets
t	time (s)
t_{cb}	column fracture time of liquid jet (s)
T	temperature (K)
u_i	instantaneous gas velocity vector (m/s)
U_g	magnitude of gas velocity (m/s)
U_i	mean gas velocity vector (m/s)
v_i	instantaneous particle velocity vector (m/s)
v_i^d	velocity vector of droplet (m/s)
v_i^s	velocity vector of dust particle (m/s)
V_{rel}	relative velocity of droplet for surrounding gas (m/s)
$V_{g,th}$	gas throat velocity (m/s)
We	Weber number (dimensionless)
x_i	position vector (m)
z	distance from Venturi entry (m)
z_{th}	distance from injection point (mm)

Greek letters

ϵ	turbulent energy dissipation rate (m^2/s^3)
ϕ	temporary variable for gas (=1, u_i, T, k, or ϵ)
Γ_φ	effective viscosity for φ
η_t	collection efficiency of a single droplet (dimensionless)
μ	viscosity coefficient of gas (Pa s)
μ_0	mean for diameter of dust particles (m)
μ_d	viscosity coefficient of droplet (Pa s)
ρ	gas density (kg/m^3)
ρ_d	droplet density (kg/m^3)
ρ_s	density of dust particle (kg/m^3)
σ_0	standard deviation for diameter of dust particles (dimensionless)
σ_d	surface tension coefficient of droplet (N/m)
τ	particle relaxation time (s)
ψ_c, ψ_c'	inertial impaction parameter (dimensionless)

Subscripts

d	droplet
i or j	tensor notation (1, 2, or 3)
p	particle (dust particle or droplet)
s	dust particle

Superscripts

$\overline{(\,)}$	density-averaged
$(\,)'$	fluctuating

optimum design is to achieve the maximum collection efficiency with the minimum pressure drop. There has been much research done to predict the performance but the flow in a Venturi scrubber is very complex: the dispersed three-phase mixture of gas, droplets, and dust particles. Interactions between gas and liquid droplets, atomization of the liquid jet, droplet breakup and collision, and interactions between liquid droplets and dust particles (collision and capturing) also occur. Due to these complex phenomena, the experimental correlations or simple models have been used so far to predict the performance [3]. These methods have limits on the performance prediction when the Venturi geometry or the operation condition changes.

In this paper, the dispersed three-phase flow of the Venturi scrubber was analyzed numerically using the Eulerian–Lagrangian method and modelling of the complex phenomena one was done one by one. The gas was assumed to be a continuum while liquid droplets and dust particles were treated as discrete entities. Atomization of the liquid jet, interaction between gas and liquid droplets, dust capture of liquid droplets, droplet breakup and collision, and droplet deformation by aerodynamic force were all taken into account by making each numerical model.

2. Literature review

Much research has been done to predict the pressure drop and collection efficiency of Venturi scrubbers. Calvert [4] suggested a prediction model for the pressure drop for the first time. With the assumption that droplets achieve the gas velocity by the end of the Venturi throat, the pressure drop was derived from Newton's law describing the force required to change the momentum of the droplets. Calvert [4] also developed a mathematical model to predict collection efficiency. The collection efficiency was obtained from mass balance for dust where the amount of removed dust per droplet was determined from the

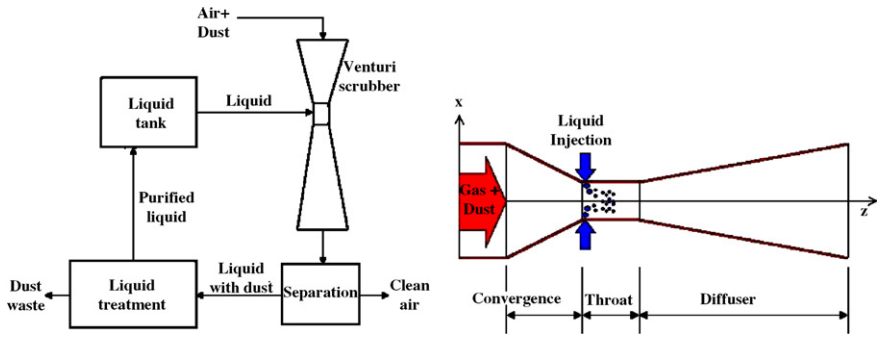

Fig. 1. System of Venturi scrubber.

correlation of target efficiency as suggested by Walton and Woolcock's experiment [5].

Boll [1] improved the mathematical model for pressure drop by including the accelerational pressure drop of the gas and the frictional pressure drop. It was comprised of simultaneous equations of drop motion, momentum exchange, and particle impaction on drops. Azzopardi et al. [6] accounted for entrainment and deposition of droplets and growth of the gas boundary layer in the diffuser in order to predict the pressure drop profiles correctly. From this study the over-recovery of pressure provided by the earlier models was explained correctly by the growth of the gas boundary layer in the diffuser section. Liquid film characteristics in a Venturi scrubber were examined experimentally by Viswanathan [7]. An annular two-phase flow model was also developed for the accurate prediction of the pressure drop. This model used a film-flow correlation to predict the liquid film thickness.

It was emphasized in Boll's study [1] that both the spatial distribution of droplets and the drop size have great effect on the collection efficiency. Spacial distribution of droplets started to be studied to improve the prediction model for collection efficiency. Taheri and Sheih [8] predicted the collection efficiency by solving the diffusion equations for both droplets and particles. The effect of the liquid distribution was also studied on collection efficiency but Boll [9] pointed out that their model did not consider the effects of initial transverse liquid momentum. Ananthanarayanan and Viswanathan [10] developed a two-dimensional model to predict the spatial distribution of droplets and the collection efficiency, where an experimental correlation was used to calculate penetration length of the injected liquid. Gonçalves et al. [11] studied the atomization of the liquid jets injected transversally to a gas stream in a Venturi scrubber. A mathematical model was developed to predict the trajectory, breakup and penetration of the liquid jets. With this model for liquid jet dynamics, Gonçalves et al. [12] calculated the spatial distribution of droplets for the case where liquid was injected through a single orifice in a rectangular Venturi scrubber.

3. Eulerian–Lagrangian approach

Gas containing dust particles enters the Venturi scrubber from the inlet, and the liquid jets are atomized into small droplets after being injected through the throat orifices. As the dust particles and the droplets move separately as a lot of discrete entities, the motion of these particles (dust and droplet) is analyzed using the Lagrangian approach in which each individual particle is tracked. The gas flow, meanwhile, is solved with the Eulerian method where gas acts as continuum.

3.1. Eulerian approach for gas flow

The gas flow is solved using the Eulerian approach by using Reynolds averaged Navier-Stokes (RANS) equations and standard $k-\epsilon$ turbulence equations. The governing equations for a gas are driven by several assumptions: (1) gas is a viscous Newtonian fluid; (2) the loading ratio of dust is very low and so the interaction between dust and gas is negligible; (3) as gas and liquid (or droplets) have the same temperature, mass exchange and heat exchange between the two phases is not considered; (4) gas turbulence is isotropic.

The governing equations are written in the following simple tensor form. Details can be found elsewhere [13].

$$\frac{\partial}{\partial t}(\rho\phi) + \frac{\partial}{\partial x_j}(\rho u_j \phi) = \frac{\partial}{\partial x_j}\left(\Gamma_\phi \frac{\partial \phi}{\partial x_j}\right) + S_\phi + S_{\phi,\mathrm{p}} \tag{1}$$

Under the above assumptions, the source terms, due to interaction with droplets, are added as $S_{\phi,\mathrm{p}}$ in the above momentum and $k-\epsilon$ turbulence equations, but the ones due to dust particles are excluded. The terms are expressed respectively as follows [13].

$$S_{u_i,\mathrm{p}} = -\frac{1}{\mathrm{d}V}\sum_{p\in(i,j,k)} m_\mathrm{p} N_\mathrm{p}\left(\frac{U_i + u_i' - v_i}{\tau}\right) \tag{2}$$

$$S_{k,\mathrm{p}} = -\frac{1}{\mathrm{d}V}\sum_{p\in(i,j,k)} m_\mathrm{p} N_\mathrm{p} u_i' \overline{\left(\frac{u_i' - v_i'}{\tau}\right)} \tag{3}$$

$$S_{\epsilon,\mathrm{p}} = 1.5\frac{\epsilon}{k} S_{k,\mathrm{p}} \tag{4}$$

where the particle relaxation time τ is

$$\tau = \frac{\pi}{3}\frac{\rho_\mathrm{p} \mathrm{d}_\mathrm{p}^3}{\rho A_\mathrm{p} C_\mathrm{D} |U_i + u_i' - v_i|} \tag{5}$$

The summation is over all particles located in a computational cell (i, j, k). The source terms are calculated by

the particle-source-in-cell method proposed by Crowe et al. [14].

3.2. Lagrangian approach for liquid droplets and dust particles

The motions of both liquid droplets and dust particles are simulated in the Lagrangian approach which requires the tracking of a sufficiently large number of computational particles. Each computational particle represents a number of liquid droplets or dust particles having equal locations, velocity, size, and temperature. This computational particle is called a 'parcel'. As it is impossible to track every individual particle because of the computer memory needed and the computation time, the parcels are usually used in the numerical simulation. The motion of the particles is described by the Basset–Boussinesq–Oseen (B–B–O) equation and their properties are obtained statistically. As the density of these particles is much higher than the gas density, the effect of the static pressure gradient, the virtual mass term and the Basset force can be neglected. The gravity force is also very small as compared with the aerodynamic drag force. The approximate form of the B–B–O equation for liquid droplets and dust particles is then

$$m_{\mathrm{p}}\frac{\mathrm{d}v_i}{\mathrm{d}t} = \frac{1}{2}C_{\mathrm{D}}\rho A_{\mathrm{p}}(u_i - v_i)|u_i - v_i| \tag{6}$$

The particle position can be obtained by integrating the following equation.

$$\frac{\mathrm{d}x_i}{\mathrm{d}t} = v_i \tag{7}$$

3.3. Drag coefficient and droplet deformation

There are two different kinds of particles in the Venturi scrubber flow: dust particles and liquid droplets. The dust particles are usually solid and their shape can be assumed to be spherical. The liquid droplets, however, can be deformed due to the aerodynamic force. In this numerical model, the change of drag coefficient induced by droplet deformation is taken into account.

Hsiang and Faeth [15] showed from their experiment that the drop deformation and breakup can be classified by the two dimensionless numbers of Weber and Ohnesorge.

$$We = \frac{\rho V_{\mathrm{rel}}^2 d_{\mathrm{d}}}{\sigma_{\mathrm{d}}}, \qquad Oh = \frac{\mu_{\mathrm{d}}}{\sqrt{\rho_{\mathrm{d}} d_{\mathrm{d}} \sigma_{\mathrm{d}}}} \tag{8}$$

The Ohnesorge number is less than 0.1 for the normal operation condition in Venturi scrubber; thus, it can be observed from the experimental regime map for droplet deformation and breakup that the regime can be divided only by the Weber number. The droplet is initially spherical and starts to deform at $We = 1$ due to the aerodynamic force. As the Weber number increases, the droplet shape changes from a sphere to a disk. At higher Weber numbers than 12, the droplet breaks up.

The drag coefficient of the deformable droplet is obtained using the experimental correlation which was suggested by

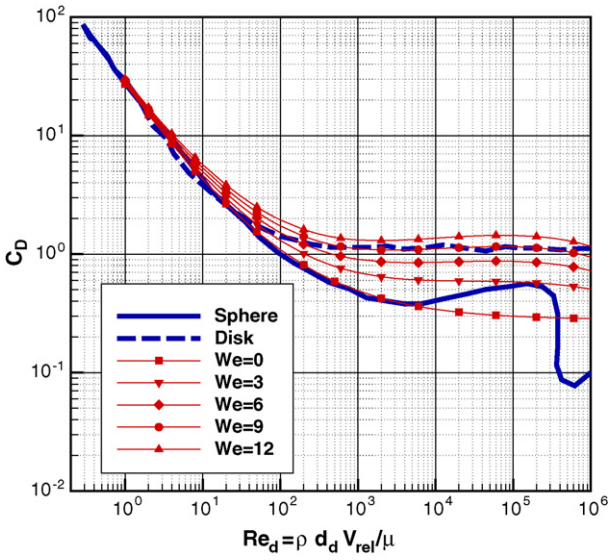

Fig. 2. Drag coefficient of deformed droplet.

Schmehl et al. [16]

$$C_{\mathrm{D}} = 0.28 + \frac{21}{Re_{\mathrm{d}}} + \frac{6}{\sqrt{Re_{\mathrm{d}}}} + We(0.2319 - 0.1579\log Re_{\mathrm{d}} + 0.047\log^2 Re_{\mathrm{d}} - 0.0042\log^3 Re_{\mathrm{d}}) \tag{9}$$

Here Re_{d} is the Reynolds number for the droplet, which is defined as follows,

$$Re_{\mathrm{d}} = \frac{\rho d_{\mathrm{d}} V_{\mathrm{rel}}}{\mu} \tag{10}$$

The drag coefficient obtained from Eq. (9) is plotted in Fig. 2. The solid line with symbols indicates the drag coefficient of the deformed droplet for several Weber numbers. As the Weber number increases, the drag coefficient moves closely from sphere to disk. The drag coefficient for $We = 12$ is used when the Weber number is over 12.

The frontal droplet area A_{p} in Eq. (6) also changes with the droplet deformation. Hsiang and Faeth [15] performed an experiment on the diameter of the deformed droplet due to aerodynamic force and suggested the following experimental correlation.

$$\frac{d_{\mathrm{def}}}{d_0} = 1 + 0.19We^{1/2} \quad (We < 100) \tag{11}$$

When the Weber number is over 100, the value for $We = 100$ is used. The frontal droplet area can be calculated from Eq. (11).

$$A_{\mathrm{p}} = \frac{\pi d_{\mathrm{def}}^2}{4} \tag{12}$$

Under the assumption that the dust particle is spherical, the following approximate drag coefficient is applied for the dust particle [13].

$$C_{\mathrm{D}} = \begin{cases} \dfrac{24}{Re_{\mathrm{s}}}\left(1 + \dfrac{1}{6}Re_{\mathrm{s}}^{2/3}\right) & Re_{\mathrm{s}} \le 1000 \\ 0.42 & Re_{\mathrm{s}} > 1000 \end{cases} \tag{13}$$

The Reynolds number for the dust particle is defined by

$$Re_s = \frac{\rho d_s |u_i - v_i^s|}{\mu} \tag{14}$$

4. Modelling for atomization of liquid jet

After liquid is injected through the throat orifice, the liquid jet forms a column. Droplets are stripped from the column by surface breakup. The liquid column then undergoes column fracture and disintegrates into large ligaments and droplets, which are divided into smaller droplets due to secondary breakup of bag, multimode and shear breakup [17].

The atomization of a liquid jet is modelled using the Lagrangian approach. The liquid jet can be divided into two parts: the liquid column and the droplets.

The liquid column is simulated using droplets with a diameter equal to the orifice. The column fracture is assumed to occur in the specified column fracture time after the jet is injected through the orifice, and the column is divided into five droplets with a root-normal size distribution [18]. This number of droplets was chosen to keep the computational cost to a manageable level even though more droplets could give slightly better resolution. The column fracture time is determined from Wu et al.'s [17] experiment and is defined by

$$t_{cb} = 3.44 \frac{d_0}{U_g} \sqrt{\frac{\rho d}{\rho}} \tag{15}$$

Besides the column fracture, the droplets are also created from the jet by the shear action of aerodynamic force. This breakup mechanism is named the surface breakup of the liquid column. It is modelled using the Reitz's wave instability model [19]. Both of the explained breakups, for the liquid column, are called the primary breakup.

Secondly, there is a breakup model for droplets that are produced due to the primary breakup. The droplets generated by the primary breakup undergo a secondary breakup in the characteristic breakup time later [20]. If the Weber number exceeds the critical point, each droplet is separated into five smaller droplets. The size of the produced droplets is assumed to follow the root-normal size distribution [15]. Details for this atomization model are explained elsewhere [21].

5. Modelling for capture of dust particle by droplet

Dust particles are absorbed into droplets through collision between two phases in the Venturi scrubber. The collision occurs by three mechanisms: inertial impaction, interception, and Brownian diffusion. The size of the dust particles that the device can treat is approximately between 0.5 and 10 μm. As Brownian diffusion is dominant below 0.1 μm, the collision between dust particles and droplets takes place mainly through inertial impaction.

In this paper the target efficiency, which means the collection efficiency of a single droplet, is used to model the capture of a dust particle by a droplet. Walton and Woolcock [5] carried out the experiment for target efficiency by inertial impaction and an experimental correlation was derived from the data [4].

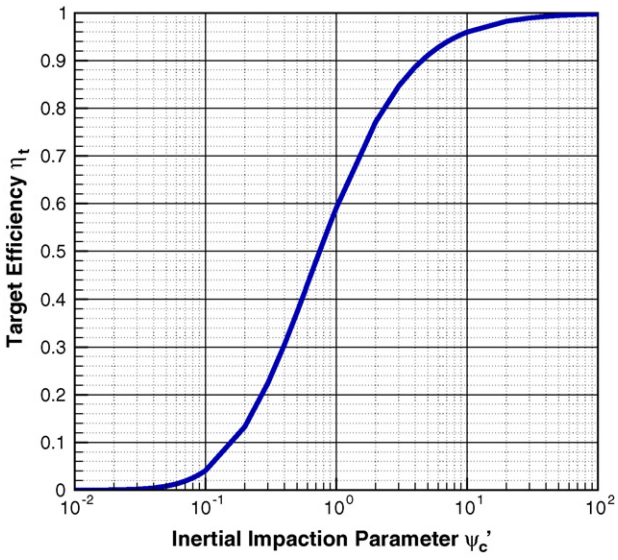

Fig. 3. Target efficiency of a single droplet.

$$\eta_t = \left(\frac{\psi_c}{\psi_c + 0.7} \right)^2 \tag{16}$$

Here, the inertial impaction parameter ψ_c, is defined by

$$\psi_c = \frac{\rho_s d_s^2 |u_i - v_i^d|}{9 \mu d_d} \tag{17}$$

Mohebbi et al. [22] induced a more precise experimental correlation for target efficiency. The graph for the target efficiency versus the inertial impaction parameter is plotted in Fig. 3. The correlation was applied to the model for capture of dust particles by droplets.

$$\eta_t = \left(\frac{\psi_c'}{\psi_c' + 1} \right)^r \tag{18}$$

where

$$r = 0.759 \psi_c'^{-0.245}, \qquad \psi_c' = \frac{\rho_s d_s^2 |u_i - v_i^d|}{18 \mu d_d} \tag{19}$$

Capturing of a dust particle by a droplet is calculated as follows. It is assumed that collision between dust particles and droplets occurs only if they exist in the same computational cell. As shown in Fig. 4, let us put M droplet parcels and N dust parcels in the same computational cell. If all droplets and dust particles are uniformly distributed throughout the computational cell, the number of dust particles that one droplet parcel captures from collision between one droplet parcel and one dust parcel, can be obtained.

$$N_{cap} - \eta_t \frac{\pi}{4} d_{def}^2 |v_i^s - v_i^d| \frac{N_s N_d}{dV} \tag{20}$$

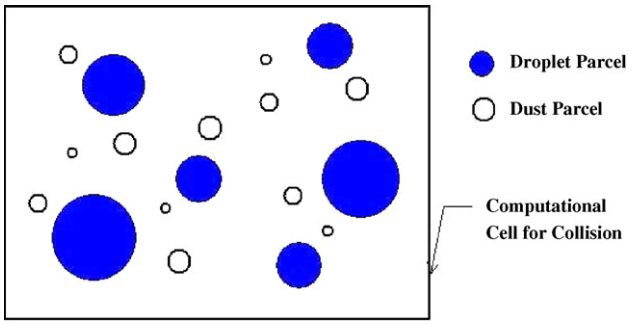

Fig. 4. Collision between droplets and dust particles in a computational cell.

The total number of dust particles that all the droplets can absorb in a computational cell is determined as below.

$$N_{\text{cell}} = \sum_{m=1}^{M}\sum_{n=1}^{N} N_{\text{cap}} \tag{21}$$

6. Numerical simulation

In this section the numerical simulation process is explained for the dispersed gas-droplet-dust particle flow in a Venturi scrubber. The process is illustrated in Fig. 5. At first, the gas-only flow field was obtained by the RANS and $k-\epsilon$ equations. These equations were solved in the finite volume approach with the SIMPLE algorithm. Next the motion of the droplets and dust particles was computed on the basis of the converged gas flow field. New droplets were injected from the throat orifice and new dust particles entered the Venturi scrubber from its inlet. Particles that left the Venturi scrubber were removed from the computation. In the case where droplets or dust particles collided with the wall, they were treated as rebounding with perfect elasticity. All the particles that existed within the device were transferred through the aerodynamic force and the turbulent dispersion, and their new positions were determined by integrating Eq. (7). Breakup and collisions of droplets were calculated at their new positions [21]. Grazing collisions and coalescence were considered to be the outcomes of the collisions, just in the same way as the KIVA code. Atomization of the liquid jet and capture of dust particles by droplets were also simulated in this step by applying the models developed here.

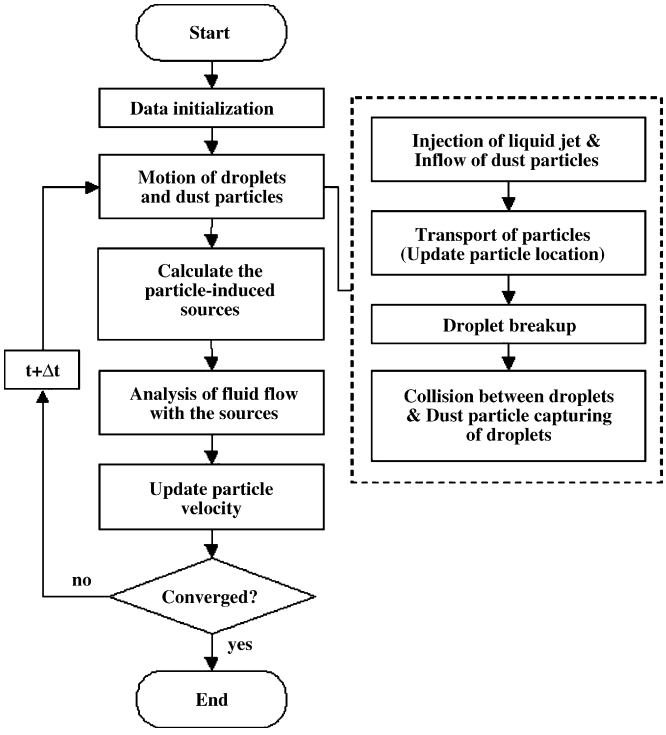

Fig. 5. Flow chart for three-phase flow simulation of Venturi scrubber.

As a third step, the particle-induced sources for momentum, turbulent kinetic energy and turbulent dissipation energy rate were calculated over each computational cell using Eqs. (2)–(4). The sources could be induced from droplets and dust particles, but as the mass flow rate of dust particles is very low and so the interaction between gas and dust particles may be negligible, only the source terms due to droplets were included. After this step, the gas flow had to be solved again with the particle-induced sources newly calculated. Finally, velocities of all the particles were updated by solving Eq. (6) using the finite difference approach. This process had to be iterated until the solution converged.

The KIVA code was used to simulate this three-phase flow and modified to include the models developed in this study.

7. Results and discussion

Numerical analysis was carried out for the circular Venturi scrubber on which Haller et al. [23] conducted an experiment. The geometry of the device is outlined in Fig. 6. The gas containing the dust particles flowed upward and the water, as scrubbing liquid, was injected through twelve concentrically arranged orifices, each 2.5 mm in diameter. As the liquid was injected towards the center, the droplets collided with each other around the center of the throat. To take this collision into account, the three-dimensional, whole flow field of the Venturi scrubber was computed, as the computational mesh is shown in Fig. 6.

The inflow velocities of the gas were limited to 50, 70, and 100 m/s and the liquid-to-gas volume flow ratio ranged from 0.55 to 2.75 l/m^3. Quartz (SiO_2) was used as the dust particle and its flow rate was fixed at 5 e-7 kg/s. As the log-normal distribution is frequently used to represent the size of the solid particles [24], it was assumed in this numerical simulation that the size of the dust particles could be represented with the log-normal distribution. The mass distribution function is given by

$$f(d_s) = \frac{1}{\sqrt{2\pi}\sigma_0 d_s}\exp\left[-\frac{1}{2}\left(\frac{\ln(d_s)-\mu_0}{\sigma_0}\right)^2\right] \tag{22}$$

Here μ_0 and σ_0 are the mean and standard deviations for the diameter of the dust particles, which are obtained from

$$\mu_0 = \ln(D_M), \qquad \sigma_0 = \ln\left(\frac{D_{84\%}}{D_M}\right) \tag{23}$$

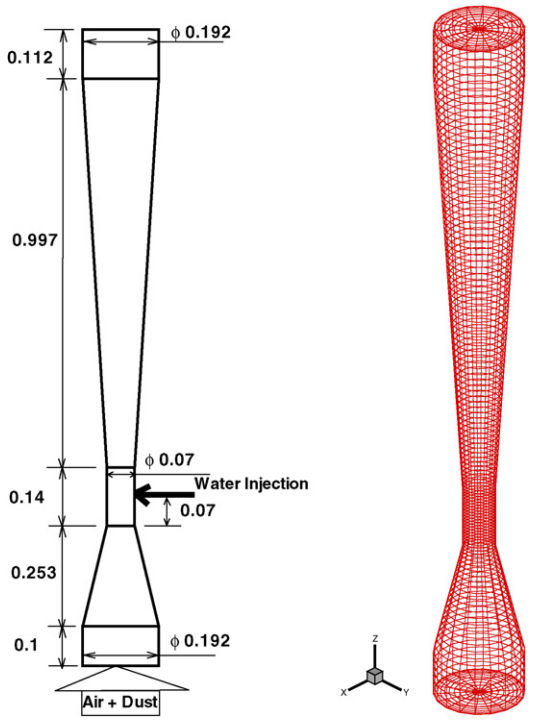

Fig. 6. Geometry and computational mesh of circular Venturi scrubber (UNIT:m).

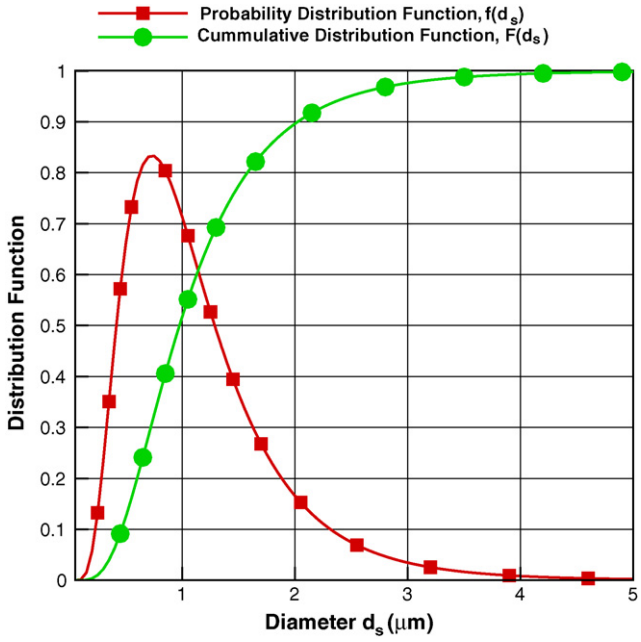

Fig. 7. Log-normal size distribution function for dust particles.

where the median diameter D_M is defined as the particle diameter for which the cumulative distribution is 0.5 and $D_{84\%}$ is the diameter corresponding to the 84th percentile on the function. The values of D_M and $D_{84\%}$ are 1.0e−6 and 1.75e−6m, respectively. This lognormal size distribution for the dust particles is plotted in Fig. 7.

The dispersed gas–liquid–dust particle flow was simulated numerically for the circular Venturi scrubber and the result is shown in Fig. 8. The throat velocity of the gas was 70 m/s and the liquid-to-gas volume ratio (or loading ratio) was 1.1 l/m^3. The dust particles entered the device with uniform spatial distribution and the liquid was injected from 12 orifices. The liquid was atomized after injection and captured the dust particles through the inertial impaction mechanism.

The contour of the gas velocity is displayed in Fig. 8(b) and (c) are for the three-phase flow and the gas-only flow respectively. In the Venturi throat, the gas velocity was reduced in the middle region between the wall and the axis as compared with the gas-only flow. This is clearly shown in Fig. 9. Most of the

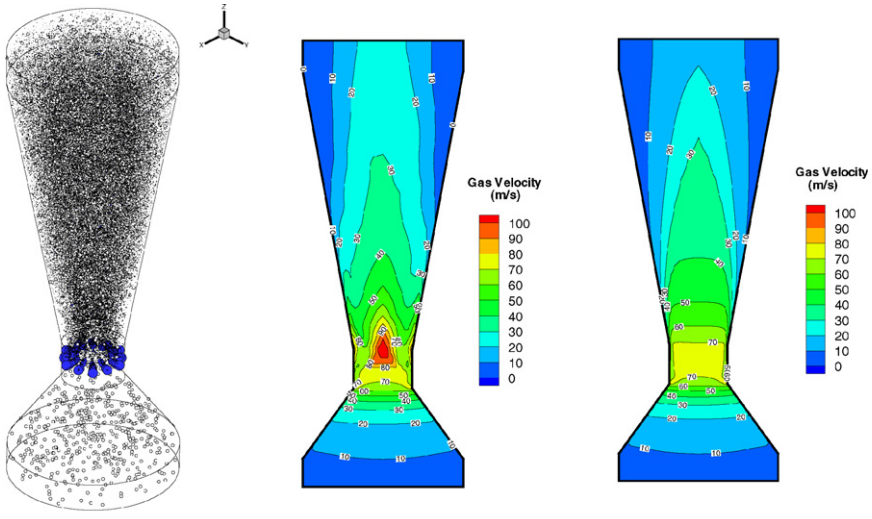

(a) Distribution of droplets and dust particles

(b) Gas velocity for three-phase flow

(c) Gas velocity for gas-only flow

Fig. 8. Numerical simulation for circular Venturi scrubber when $V_{g,th}$ = 70 m/s and l/g = 1.1 U/m^3 (Scaled by X to Z ratio = 3).

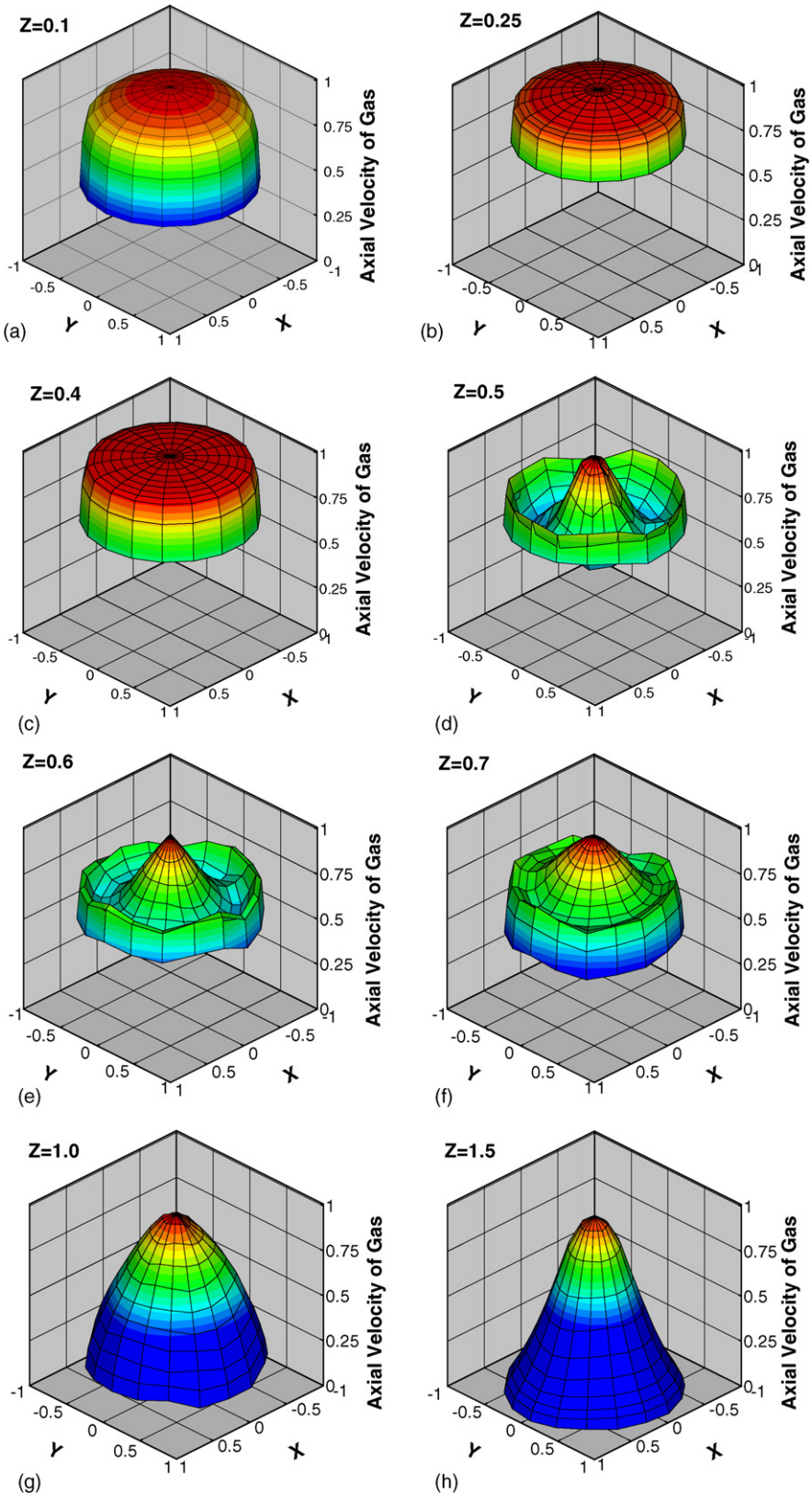

Fig. 9. Profiles of gas velocity in axial direction when $V_{g,th} = 70$ m/s and $l/g = 1.1$ l/m^3 (each axes are normalized with its own maximum value).

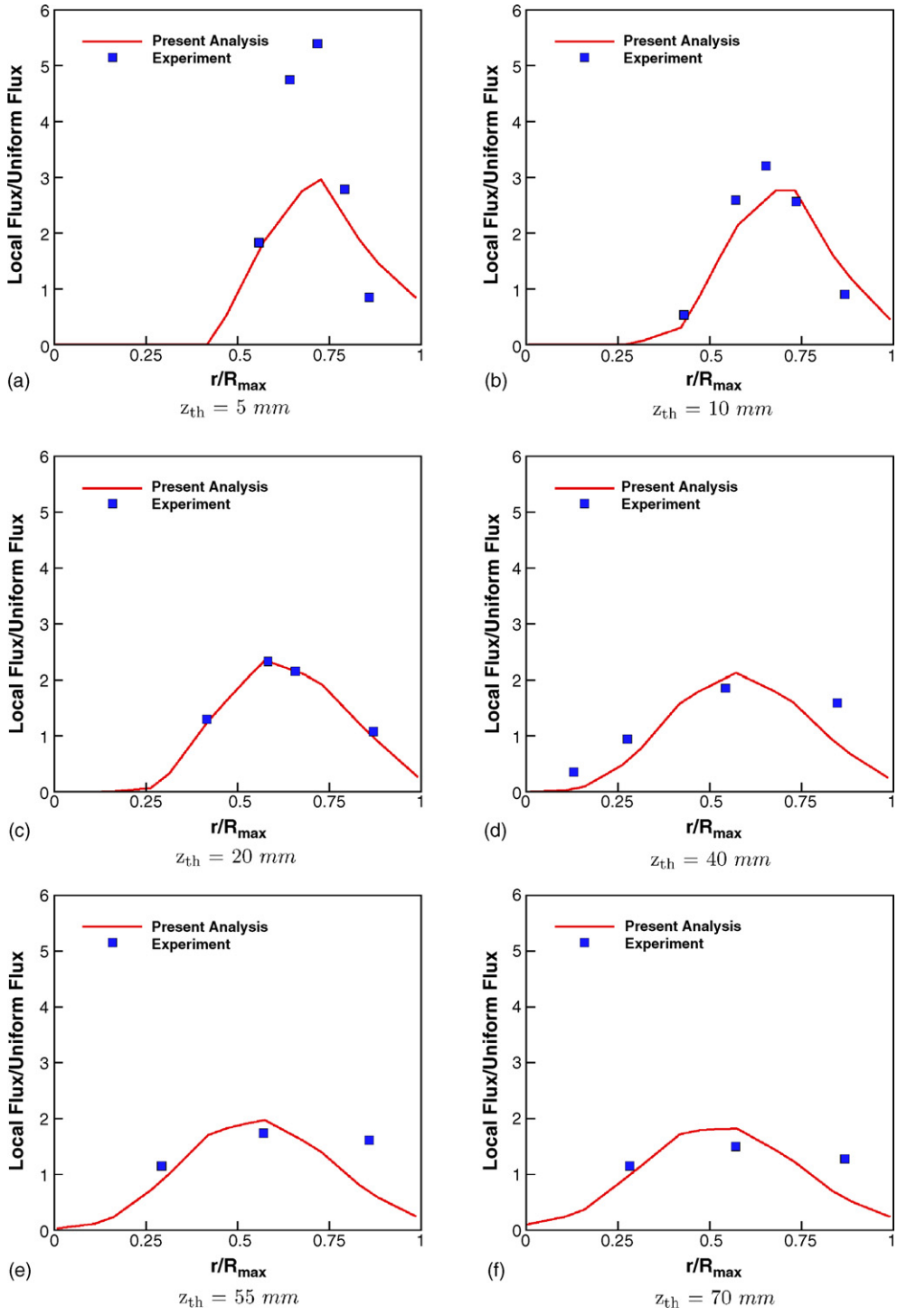

Fig. 10. Liquid flux distribution in Venturi throat when $V_{g,th}$ = 70 m/s and l/g 1.1 l/m^3: (●) experimental data [23]; (solid line) present analysis.

droplets injected from the orifices existed in the middle region, which can be identified from Fig. 10, and the droplets achieved almost their maximum velocities within the throat, as observed in Fig. 11. Therefore, it was deduced that droplets were accelerated by receiving the momentum of the gas in the middle region. The reduction of the gas velocity in the middle region of the Venturi throat can be explained from this fact. As a result, the center part of the gas in the Venturi throat had to have a higher velocity in the three-phase flow than in the gas-only flow, in order to satisfy mass conservation.

7.1. Pressure drop

The pressure drop in the Venturi scrubber is caused by mechanisms such as (a) momentum change of the gas; (b) momentum change of the droplets; (c) friction; (d) momentum change of the

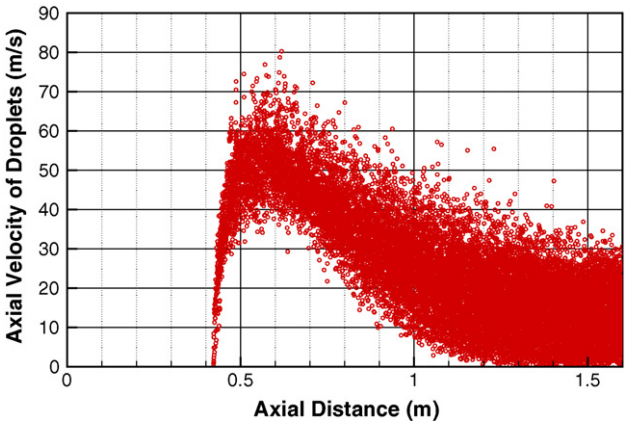

Fig. 11. Droplet velocity in axial direction when $V_{g,th} = 70$ m/s and $l/g = 1.1$ l/m^3.

liquid film; and (e) gravity [3]. Azzopardi et al. [6] examined the relative importance of the above five components of pressure drop. They concluded from their study that the acceleration and deceleration of the gas and droplets were the most important components, while film momentum and gravitation had only small effects on pressure drop. As implied in Viswanathan's study [7], liquid film needs to be taken into consideration to predict pressure drop more accurately. However, the effect of liquid film on pressure drop is small and it is too complex to model and simulate numerically in the three-dimensional way. Because of this reason, the liquid film was not considered in this paper.

The pressure drop calculated from this numerical analysis was compared with Haller et al.'s experimental data [23]. The gas velocity at the throat, $V_{g,th}$, was 70 m/s. The pressure drop was calculated from the static pressure difference between the inlet and the outlet of the Venturi scrubber. It is shown from Fig. 12 that the overall pressure drop was about 15% lower than the experiment at the liquid-to-gas volume ratio $l/g = 1.1$, 1.65, and 2.2 l/m^3, but the overall numerical result gave comparable agreement with the experiment.

These discrepancies on pressure drop can be explained from droplet size and liquid film. Table 1 shows the Sauter mean diameter (SMD) value for each operation condition. One column of SMD values (Num.) was computed from this numerical simulation and the other (Boll) was calculated from the following Boll's correlation [1].

$$D_{32} = \frac{4.2 \times 10^{-2} + 5.65 \times 10^{-3}(l/g)^{1.922}}{V_{rel}^{1.602}} \quad (24)$$

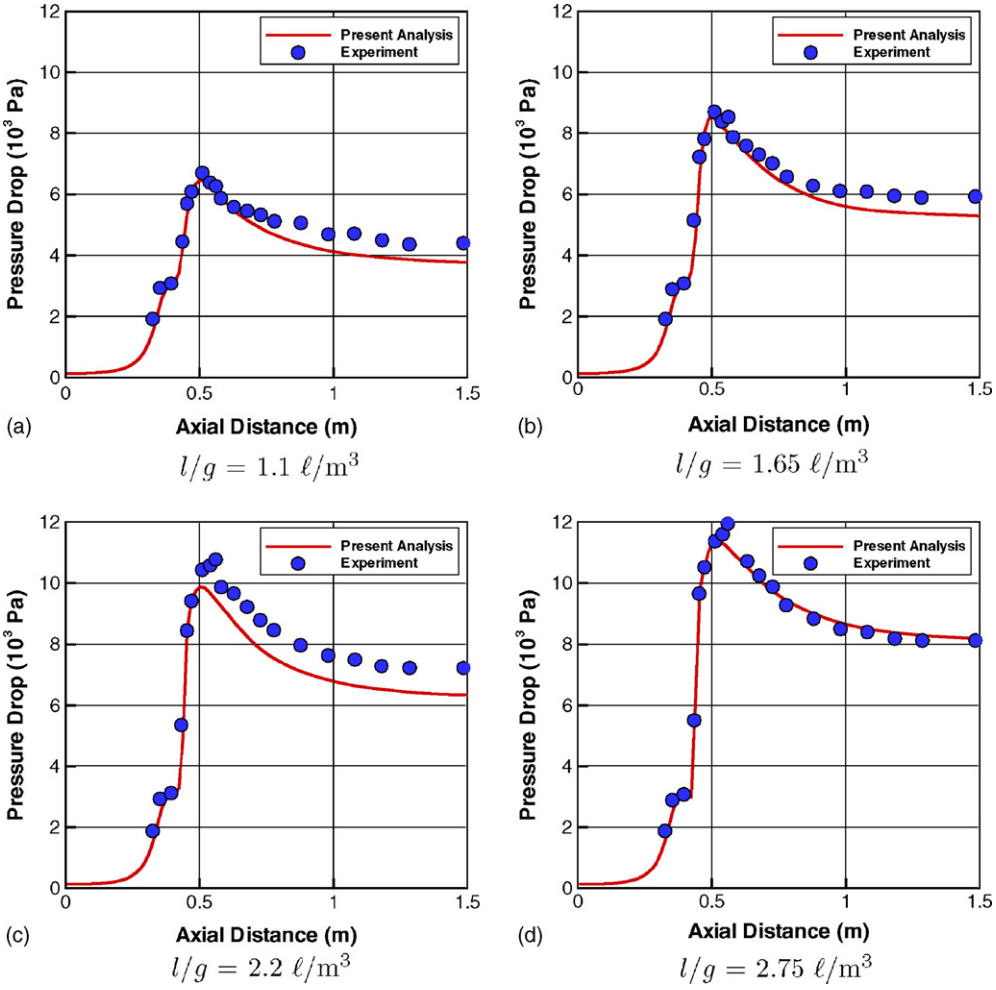

Fig. 12. Pressure drop vs. axial distance when gas throat velocity = 70 m/s: (●) experimental data [23]; (solid line) present analysis.

Table 1
Experimental and numerical results for droplet diameter, target efficiency and collection efficiency

Gas throat velocity (m/s)	Loading ratio (l/m^3)	SMD (μm)		Target efficiency (%)			Collection efficiency (%)		
		Boll	Num.	Boll	Num.	Error	Exp.	Num.	Error
	0.55	83	192	88.9	74.4	16.3	83.4	83.6	0.2
	1.1	91	182	87.8	75.6	13.9	95.0	84.6	10.9
50	1.65	104	169	85.9	77.2	10.1	97.2	89.0	8.4
	2.2	122	168	83.5	77.4	7.3	97.5	91.5	6.2
	2.75	144	171	80.5	77.0	4.4	97.6	92.8	4.9
	0.55	48	98	95.9	90.8	5.3	94.0	92.6	1.5
	1.1	53	90	95.4	91.6	4.0	98.0	95.8	2.2
70	1.65	61	81	94.6	92.6	2.2	98.9	96.5	2.4
	2.2	71	85	93.6	92.1	1.6	99.4	97.2	2.2
	2.75	84	90	92.3	91.6	0.7	99.2	97.7	1.5
	0.55	27	55	98.6	96.9	1.8	97.3	96.7	0.6
	1.1	30	51	98.5	97.1	1.4	99.1	99.5	0.4
100	1.65	34	49	98.2	97.3	1.0	–	99.5	–
	2.2	40	52	97.8	97.1	0.8	–	99.7	–
	2.75	47	68	97.4	96.0	1.4	–	99.7	–

As concluded in the study of Alonso et al. [25], the above equation correlates well with the SMD of liquid drops injected from the Venturi scrubber. It is seen from Table 1 that the SMD of numerical simulation was larger than the SMD of Boll's correlation. It means that the number of droplets was smaller in this numerical simulation than in the experiment. The resultant large droplets had larger Stokes numbers. If the Stokes number is large, droplets have a large momentum response time. Thus, the droplet velocity will be less affected during its passage through the Venturi. This small number and the large size of the droplets in this simulation seemed to cause lower pressure drop in the Venturi throat by getting less momentum from the gas.

Liquid film also appeared to work as one of the causes that made some discrepancies in the pressure drop. Liquid film is related to many complex phenomena; especially, deposition and entrainment of droplets, wall friction increase due to film roughness, and momentum exchange of liquid film, are very important [7]. If it is assumed that the gas momentum saved due to deposition cancels out the momentum loss due to entrainment, then the two other factors, film roughness and film momentum, will cause the pressure loss. Because this numerical model did not consider these liquid film phenomena, it predicted a little lower pressure drop in the throat and diffuser than the experiment.

As shown in Fig. 12, the pressure dropped continuously up to the liquid injection point of $z = 0.42$ and it stayed nearly constant for the short distance of the throat. The major component of the cause of pressure drop in this region was thought to be the acceleration of the gas. Right after the injection point, the pressure drop suddenly increased. As shown in Fig. 11, the injected droplets achieved almost their maximum velocities within the throat ($0.42 < z < 0.5$). Meanwhile there was no gas acceleration in the throat and the friction was too small to cause such a large pressure drop. It could be said, therefore, that the sudden increase of pressure drop resulted from the acceleration of the droplets. The momentum loss of the gas, owing to the droplet acceleration, can be identified in Fig. 9(d). Before the liquid was injected, the profile of the gas velocity was nearly uniform, as in Fig. 9(c). However, in Fig. 9(d), the gas velocity decreased in the middle area between the wall and the axis, where most of the droplets existed.

Finally, the pressure in the diffuser was recovered to some extent. The pressure recovery was slightly over-predicted when compared with the experiment. There could be two reasons for this. One is that there was less wall friction caused by not regarding the liquid film and the other is that there were larger droplets, than in the experiment, obstructing the pressure recovery by dragging the surrounding gas. Although there was a little disagreement on pressure drop with the experiment, this model gave better coincidence than the previous models. It appeared to come from the good prediction on growth of the gas boundary layer whose importance on the correct prediction of the pressure recovery in the diffuser was emphasized by Azzopardi et al. [6]. It can be observed in Fig. 9(g) and (h) that the gas boundary layer grew a lot in the diffuser.

The change of pressure drop due to the change of gas velocity in the throat and the liquid-to-gas volume ratio is shown in Fig. 13. As the gas velocity and liquid-to-gas ratio increased, the pressure drop became higher. Especially when the gas velocity was high, the pressure drop by the liquid-to-gas ratio had a higher rate of increase.

7.2. Collection efficiency

The collection efficiency of gas cleaning equipments can be defined in two different ways: overall collection efficiency and grade efficiency. The overall collection efficiency is defined by the mass ratio of the removed dust particles to the total inflow mass of dust particles. The other definition, grade efficiency, is defined as the collection efficiency for the dust particles of a specific size.

As the spatial distribution or mass flux distribution of the droplets has a great effect on the collection efficiency, the flux distribution was at first calculated and compared with the experimental data in Fig. 10. The throat velocity of gas was 70 m/s

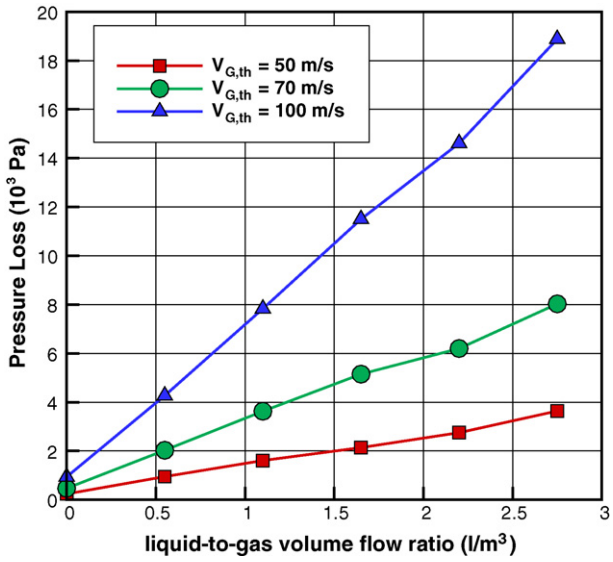

Fig. 13. Pressure loss vs. liquid-to-gas volume ratio l/g for various gas velocities $V_{g,th}$.

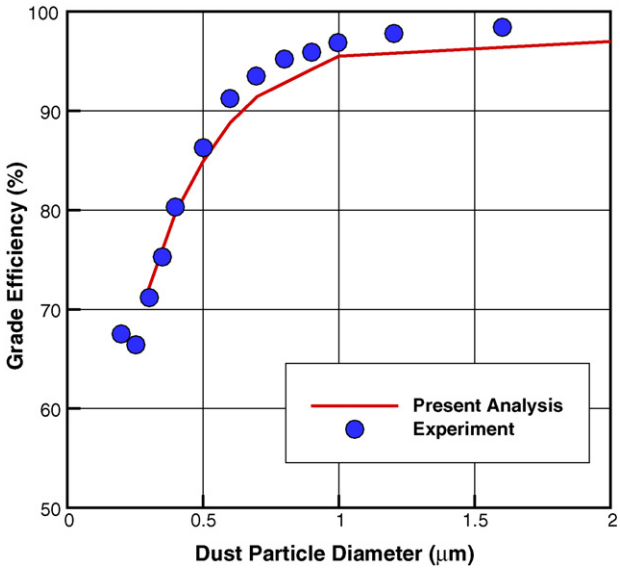

Fig. 14. Grade efficiency when $V_{g,th} = 70$ m/s: (●) experimental data [23]; (solid line) present analysis.

and the loading ratio was 1.1 l/m^3. The liquid mass flux was calculated at distances of 5, 10, 20, 40, 55, and 70 mm from the injection orifices. The mass flux was defined as total mass of droplets passing through local area, ΔA, between r and $r+\Delta r$ for time Δt, divided by the local area and the time. The uniform mass flux was over the whole cross-sectional area at each z_{th}. The position of $z_{th} = 70$ indicates the throat end. The x-axis of the graph means the radial distance from the throat center at a cross section; $r = 0$ and $r = R_{max}$ are the center and wall of the throat, respectively.

The injected liquid showed a high concentration at the near wall right after injection and the liquid flux distribution became more uniform downstream due to the inertial momentum of the injected liquid and the turbulent dispersion of the droplets. Though the numerical results had some deviation from the experiment, the maximum flux position coincided with the experiment data. From this viewpoint the numerical analysis gave reasonable flux distribution.

The grade efficiency was obtained from this numerical simulation and the accuracy was evaluated by comparing with the experimental data in Fig. 14. The results were computed for the case of $V_{g,th} = 70$ m/s and $l/g = 0.55$ l/m^3. The grade efficiency fell rapidly under 1 μm. This phenomenon was thought to be caused by the reduced inertia of a small dust particle under 1 μm. Thus, the size distribution of the dust particles should be taken into consideration to predict the collection efficiency accurately.

The average droplet SMD was also computed at the throat end for various gas velocities and loading ratios. The results are plotted in Fig. 15. As already mentioned in Section 7.1, the Boll's correlation for SMD, Eq. (24), agrees well with the experiment. The SMDs calculated by this new model, therefore, were compared with those from the Boll's correlation in Table 1.

The SMDs from the numerical simulation were much larger than the Boll's ones. This gap was believed to result from the inaccuracy of the root-normal size distribution used in the model for atomization of a liquid jet. In both cases, the SMD became smaller with the increase of the gas throat velocity. The same trend was observed in Wu et al.'s [26] experiment on a liquid jet in crossflow but as for the increase of the loading ratio, a different trend was found; the SMD from Boll's correlation increased, but the SMD from this model was almost constant. Let the SMD trend for this model be analyzed in more detail. The SMD decreased until $l/g = 1.5$ and remained almost constant over that ratio. Especially for the case of $V_{g,th} = 70$ and 100 m/s, the SMD increased at over $l/g = 1.5$. It was, however, observed by Wu et al. [26] that the SMD decreases with the increase of liquid injection velocity in a single liquid jet.

This opposite trend can be explained with droplet collision and droplet size. In a Venturi scrubber, the liquid is injected

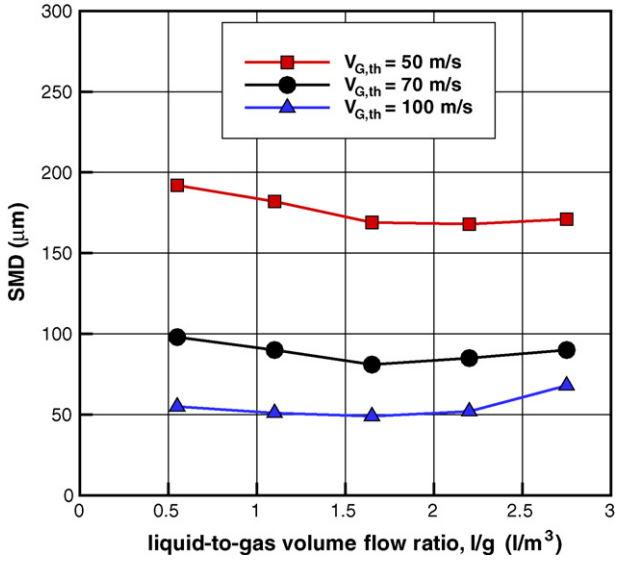

Fig. 15. Average droplet SMD at Venturi throat end.

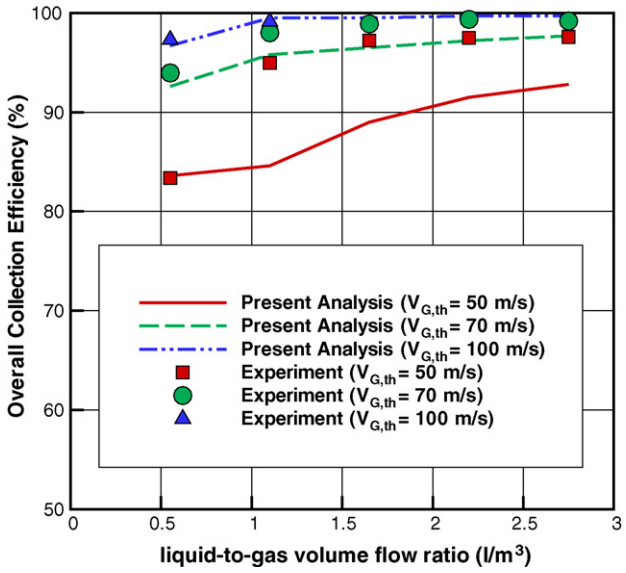

Fig. 16. Overall collection efficiency (symbols: experimental data [23], lines: present analysis).

toward the center from many nozzles. As droplets become denser with the increase of the loading ratio, more droplets collide with each other and the SMD increases by means of coalescence. The SMD of this numerical simulation, however, decreased at lower loading ratios. It seemed to result from the fact that the droplet size was much larger than in the experiment and thus the number density was too low to collide with each other actively. As the loading ratio increased more, the number density increased and the SMD increased. It could be concluded from this analysis that in order to predict droplet size correctly, not only should the proper drop size distribution be used, but the collision between droplets should be considered.

Finally, the change in the overall collection efficiency was investigated for several gas velocities and loading ratios. The numerical results shown by the lines are compared in Fig. 16 with the experimental data (symbols). At $V_{g,th} = 50$ and 70 m/s, this numerical model gave much lower collection efficiency than the experiment, and as the gas throat velocity and the loading ratio increased, the prediction was closer to the experiment.

This prediction tendency for the overall collection efficiency was likely related to the inaccurate droplet size of this model. In order to explain the role of droplet size on collection efficiency, SMD, target efficiency, and collection efficiency are summarized in Table 1 for the two cases: this numerical simulation and Boll's correlation. The target efficiency was calculated with Eq. (18) using each SMD for the two cases and the collection efficiency was brought from the same data used in Fig. 16.

It can be found from Eq. (19) and Fig. 3 that the target efficiency is in inverse proportion to SMD. The target efficiencies, therefore, were lower than those calculated with the Boll's SMD because of the larger SMD predicted by this model, but the error gap between the two cases narrowed from about 10 to 1% with the increase of $V_{g,th}$. At $V_{g,th} = 50$, the target efficiency was around 80 %. It can be observed from Fig. 3 that the region of this target efficiency is very sensitive to the inertia impaction parameter. Meanwhile the target efficiency for $V_{g,th} = 100$, which is over 95%, is much less sensitive. From these reasons, the numerical model gave better agreement with the experiment at higher $V_{g,th}$ and higher l/g. Accurate prediction of droplet size is very important for the correct estimation of collection efficiency, like the case of pressure drop.

8. Conclusion

A new three-dimensional numerical model has been developed to predict the pressure drop and collection efficiency of a Venturi scrubber. This new model solved the dispersed gas–liquid–dust particle flow using the Eulerian–Lagrangian approach. Change of the drag coefficient due to droplet deformation, atomization of a liquid jet in crossflow, droplet collision and breakup, interaction between gas and droplet, and poly-dispersed droplets and dust particles were all taken into account. Capturing of dust particles by droplets was modelled stochastically by using the target efficiency of a single droplet.

This newly developed model was tested with a circular Venturi scrubber and compared with the experiment. The pressure drop was a little under-predicted. The reason was understood from two facts. One was that the prediction of droplet size was inaccurate and the other was that the liquid film was not included in this model. The estimation for collection efficiency was in reasonably good agreement with the experiment but as the gas throat velocity and the liquid loading ratio decreased, the collection efficiency computed from this model was under-predicted much more than the experiment. This discrepancy was inferred to result from droplet sizes larger than in the experiment. The droplet size, therefore, was a very important parameter for the correct performance estimation of a Venturi scrubber, and it was also found that collision between droplets had an important effect on droplet size.

As a future study, in order to predict the performance of a Venturi scrubber more accurately, it is necessary to improve the new model in some aspects: (1) accurate prediction of droplet size in the model for atomization of the liquid jet and (2) consideration of a liquid film.

References

[1] R.H. Boll, Particle collection and pressure drop in Venturi scrubbers, Ind. Eng. Chem. Fundam. 12 (1) (1973) 40–50.
[2] R.A. Pulley, Modelling the performance of Venturi scrubbers, Chem. Eng. J. 67 (1997) 9–18.
[3] J.A.S. Gonçalves, D.F. Alonso, M.A. Martins Costa, B.J. Azzopardi, J.R. Coury, Evaluation of the models available for the prediction of pressure drop in Venturi scrubbers, J. Hazard. Mater. 81 (2001) 123–140.
[4] S. Calvert, Venturi and other atomizing scrubbers efficiency and pressure drop, AIChE J. 16 (3) (1970) 392–396.
[5] W.H. Walton, A. Woolcock, Aerodynamic Capture of Particles, Pergamon Press, New York, 1960.
[6] B.J. Azzopardi, S.F.C.F. Teixeira, A.H. Govan, T.R. Bott, An improved model for pressure drop in Venturi scrubbers, Trans. IChemE 69 (1991) 237–245.
[7] S. Viswanathan, Examination of liquid film characteristics in the prediction of pressure drop in a Venturi scrubber, Chem. Eng. Sci. 53 (17) (1998) 3161–3175.

[8] M. Taheri, C. Sheih, Mathematical modeling of atomizing scrubbers, AIChE J. 21 (1) (1975) 153–157.
[9] Letters to the editor AIChE J. 21 (4) (1975) 831.
[10] N.V. Ananthanarayanan, S. Viswanathan, Predicting the liquid flux distribution and collection efficiency in cylindrical Venturi scrubbers, Ind. Eng. Chem. Res. 38 (1999) 223–232.
[11] J.A.S. Gonçalves, M.A.M. Costa, P.R. Henrique, J.R. Coury, Atomization of liquids in a Pease–Anthony Venturi scrubber Part I. Jet dynamics, J. Hazard. Mater. 97 (2003) 267–279.
[12] J.A.S. Gonçalves, M.A.M. Costa, M.L. Aguiar, J.R. Coury, Atomizatin of liquids in a Pease–Anthony Venturi scrubber. Part II. Droplet dispersion, J. Hazard. Mater. 116 (2004) 147–157.
[13] A.A. Amsden, P.J. O'Rourke, T.D. Butler, KIVA-II: a computer program for chemically reactive flows with sprays, Los Alamos National Laboratory Report, LA-11560-MS, 1985.
[14] C.T. Crowe, M.P. Sharma, D.E. Stock, The particle-source-in cell (PSI-CELL) model for gas-droplet flows, J. Fluid. Eng., Trans. ASME 99 (1977) 325–332.
[15] L.P. Hsiang, G.M. Faeth, Near-limit drop deformation and secondary breakup, Int. J. Multiphas. Flow 18 (5) (1992) 635–652.
[16] R. Schmehl, G. Maier, S. Wittig, CFD analysis of fuel atomization, secondary droplet breakup and spray dispersion in the premix duct o f a LPP combustor, in: Proceedings of the 8th International Conference on Liquid Atomization and Spray Systems, Pasadena, CA, USA, 2000.
[17] P.K. Wu, K.A. Kirkendall, R.P. Fuller, A.S. Nejad, Breakup processes of liquid jets in subsonic crossflows, J. Propul. Power 13 (1) (1997) 64–73.
[18] R.K. Madabhushi, A model for numerical simulation of breakup of a liquid jet in crossflow, Atomization Spray 13 (2003) 413–424.
[19] R.D. Reitz, Modeling atomization process in high-pressure vaporizing sprays, Atom. Spray Tech. 3 (1987) 309–337.
[20] M. Pilch, C.A. Erdman, Use of breakup time data and velocity history data to predict the maximum size of stable fragments for acceleration-induced breakup of a liquid drop, Int. J. Multiphas. Flow 13 (6) (1987) 741–757.
[21] S.I. Pak, Numerical modeling for performance analysis of three-phase flow in Venturi scrubber, Doctoral thesis, KAIST, Daejeon, South Korea, 2005.
[22] A. Mohebbi, M. Taheri, J. Fathikaljahi, M.R. Talaie, Simulation of an orifice scrubber performance based on Eulerian/Lagrangian method, J. Hazard. Mater. 100 (2003) 13–25.
[23] H. Haller, E. Muschelknautz, T. Schultz, Venturi scrubber calculation and optimization, Chem. Eng. Technol. 12 (1989) 188–195.
[24] C. Crowe, M. Sommerfeld, Y. Tsuji, Multiphase Flows with Droplets and Particles, CRC Press LLC, 1998.
[25] D.F. Alonso, J.A.S. Gonçalves, B.J. Azzopardi, J.R. Coury, Drop size measurements in Venturi scrubbers, Chem. Eng. Sci. 56 (2001) 4901–4911.
[26] P.K. Wu, K.A. Kirkendall, R.P. Fuller, A.S. Nejad, Spray structure of liquid jets atomized in subsonic crossflows, J. Propul. Power 14 (2) (1998) 173–182.